

Rethinking Text-Promptable Surgical Instrument Segmentation with Robust Framework

Tae-Min Choi, and Juyoun Park, *Member, IEEE*

Abstract—Surgical instrument segmentation (SIS) is essential in computer-assisted surgeries, with deep learning methods improving accuracy in complex environments. Recently, text-promptable segmentation methods have been introduced, generating masks based on textual descriptions. However, they assume the text-described object is present and always generate an associated mask even when the object is absent. Existing methods address this by using prompts only for objects already known to exist in the scene, which relies on inaccessible information. To address this, we rethink text-promptable SIS and redefine it under robust conditions as Robust text-promptable SIS (R-SIS). Unlike previous approaches, R-SIS is a process that analyzes text prompts for all surgical instrument categories without relying on external knowledge, identifies the instruments present in the scene, and segments them accordingly. Building on this, we propose Robust Surgical Instrument Segmentation (RoSIS), an optimized framework combining visual and language features for promptable segmentation in the R-SIS setting. RoSIS employs an encoder-decoder architecture with a Multi-Modal Fusion Block (MMFB) and a Selective Gate Block (SGB) for balanced integration of vision and language features. Additionally, an iterative refinement strategy enhances segmentation masks through a two-step process: an initial pass with name-based prompts, followed by refinement with location prompts. Experiments across multiple datasets and settings show that RoSIS outperforms existing vision-based and promptable segmentation methods under robust conditions. By rethinking text-promptable SIS, our work establishes a fair and effective approach to surgical instrument segmentation.

Index Terms—Surgical instrument segmentation, Feature fusion, Iterative refinement, Robustness, Text-promptable

I. INTRODUCTION

MINIMALLY invasive surgeries [1], [2] are widely adopted due to their advantages, requiring surgeons to rely on camera-captured views instead of direct visualization. Surgical Instrument Segmentation (SIS) [3] is fundamental to enhancing surgical vision. Deep learning-based SIS methods [4]–[9] have shown promising results. However, their

This work was supported by the Technology Innovation Program (RS-2024-00443054, Development of a Supermicrosurgical Robot System for Sub-0.8mm Vessel Anastomosis through Human-Robot Autonomous Collaboration in Surgical Workflow Recognition) funded by the Ministry of Trade Industry & Energy (MOTIE, Korea).

Tae-Min Choi and Juyoun Park are with Center for humanoid research, Korea Institute of Science Technology (KIST), Seoul, South Korea (e-mail: tmchoi@kist.re.kr; juyounpark@kist.re.kr).

performance is often limited by small datasets, and they lack adaptability for human-robot interaction in robot-assisted surgeries.

To address these challenges, vision-language models have introduced text-promptable segmentation [10], [11], inspired by Referring Image Segmentation (RIS) [12], [13]. RIS enables mask generation based on text descriptions, assuming the described object exists in the image. However, this assumption leads to incorrect masks when the object is absent. Generalized Referring Expression Segmentation [14] and Robust Referring Image Segmentation [15] tackle this by first verifying object existence before segmentation.

A similar issue arises in text-promptable SIS methods. These methods generate segmentation masks based on textual descriptions, typically including the instrument's name and additional attributes provided by large language models such as GPT-4 [16]. However, they also assume that the described instrument is present, leading to incorrect masks when it is absent. Existing approaches mitigate this by only generating prompts for instruments present in the image (inaccessible information, middle row of Fig 1). However, this introduces inaccessible information during evaluation, resulting in unfair comparisons with vision-based methods. The presence or absence of an instrument is inaccessible in the real world without an additional detection process. Since such information is typically provided during training but not during evaluation or testing, using it for evaluation leads to unfair comparisons with vision-based methods that do not rely on such information.

To ensure fairness, we rethink text-promptable SIS and propose Robust text-promptable SIS (R-SIS). Unlike previous methods, R-SIS integrates text prompts for all dataset categories, regardless of their presence in the image. As illustrated in Fig. 1, previous promptable SIS methods [10], [11], [17] selectively use prompts only for objects detected in the image, relying on information unavailable to vision-based models. R-SIS eliminates this bias by incorporating negative prompts for absent objects and positive prompts for present ones, allowing the model to distinguish object presence during segmentation. We construct an R-SIS dataset using EndoVis2017 [18] and EndoVis2018 [19], ensuring comprehensive prompts for robust training and evaluation.

To validate our hypothesis, we measured the performance variations of text-promptable surgical instrument segmentation models in the previous setting (without a robust condition) and our R-SIS setting (with a robust condition). Conventional promptable SIS methods exhibit increased false positives un-

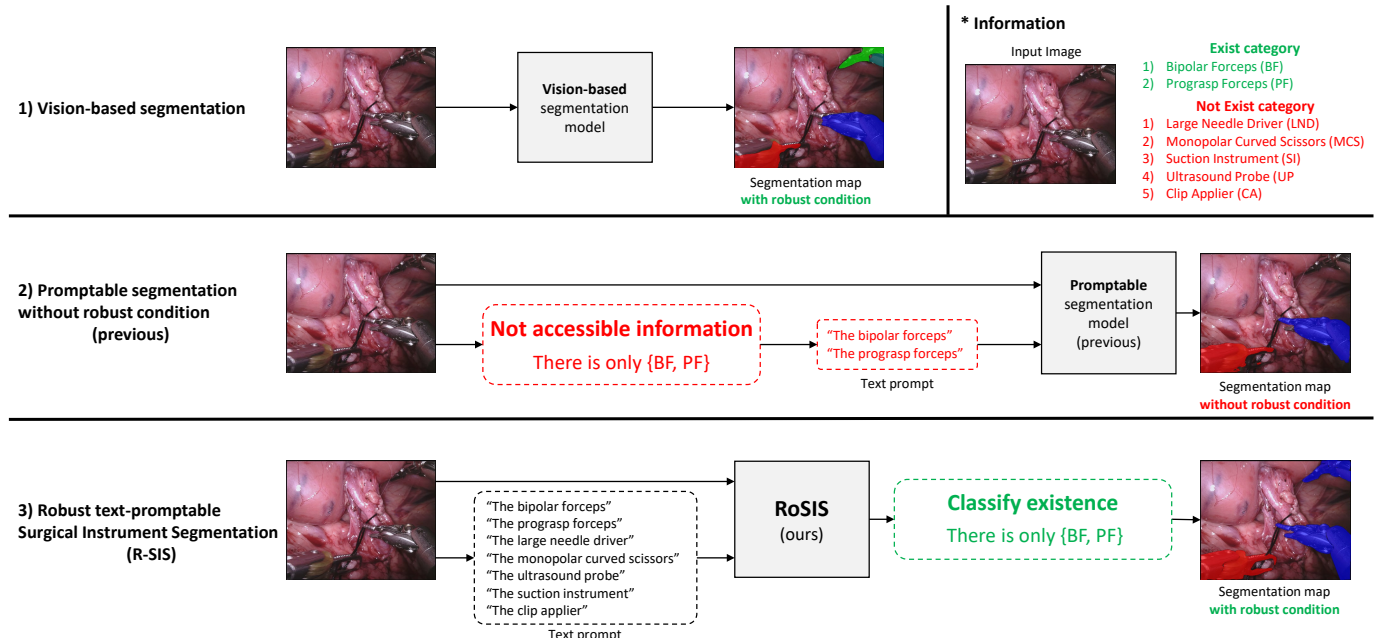


Fig. 1. Comparison of SIS method: (1) Vision-based segmentation model [4]–[7] only uses the image and generates all classes of segmentation maps; (2) Previous promptable segmentation model [10], [11], [17] uses “not accessible information” to identify categories present in the image and generates segmentation maps only for those categories. This means they are led to settings without robust conditions; (3) Our robust promptable segmentation model uses prompts for all classes, generating segmentation maps for all categories under robust conditions.

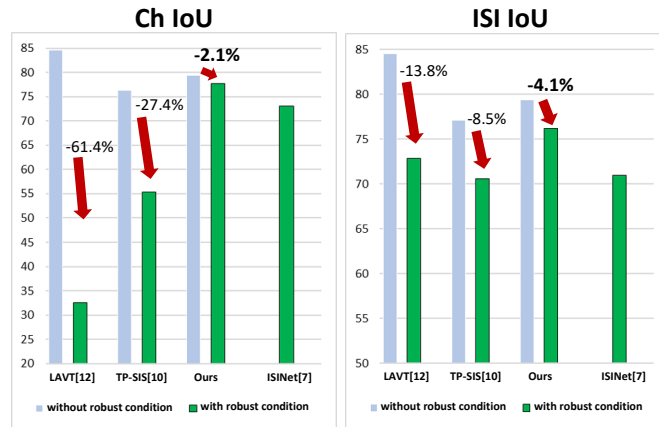


Fig. 2. Performance comparison on the EndoVis2018 dataset under with and without robust conditions. Challenge IoU (Ch IoU) is the mean IoU computed only for classes in the image, while ISI IoU measures the IoU across all classes. Existing models exhibit significant performance degradation, with dramatic drops in both Ch IoU and ISI IoU. In contrast, our robust promptable segmentation model demonstrates minimal performance degradation across both metrics and outperforms the ISINet [7], the SOTA vision-based model under robust conditions.

der the R-SIS setting, leading to performance degradation, as shown in Fig. 2. In some cases, these methods even perform worse than vision-based models that do not utilize language information. To overcome this limitation, we introduce **Robust Surgical Instrument Segmentation (RoSIS)**, an optimized framework designed for robust conditions. RoSIS incorporates two key modules: the **Multi-Modal Fusion Block (MMFB)**, which effectively integrates visual and textual features, and the **Selective Gate Block (SGB)**, which dynamically balances visual and fused features. Additionally, we propose

an **iterative refinement** strategy that enhances segmentation accuracy through a two-step process. The first step generates an initial segmentation using instrument name-based and large language model-based prompts. The second step refines the segmentation using location prompts derived from the initial prediction.

Our experiments on EndoVis2017 and EndoVis2018 demonstrate that RoSIS outperforms existing vision-based and promptable segmentation methods under robust conditions. We carefully design our evaluation process to ensure fair benchmarking and validate the effectiveness of our RoSIS compared to existing methods. Our results demonstrate RoSIS’s robustness and reliability, reinforcing the advantages of our redefined R-SIS framework for surgical instrument segmentation.

II. RELATED WORKS

A. Surgical Instrument Segmentation

SIS involves predicting the pixel-wise regions of instruments in surgical images. Early research [4], [7]–[9], [20] applied image-based segmentation methods to SIS. TernausNet [4] introduced a modified U-Net [21] architecture with pre-trained VGG11/VGG16 encoders and skip connections for precise location. ISINet [7], utilizing a Mask R-CNN [22] architecture, incorporates a temporal consistency module to refine instrument predictions across video frames. TraSeTR [20] employs a Track-to-Segment Transformer, combining query embeddings with contrastive learning for robust tracking and segmentation. MATIS [9], a video-based SIS method, uses a two-stage structure with Mask2Former [23] to generate and classify region proposals, incorporating masked and deformable attention and video transformers for temporal

consistency. S3Net [8] extends Mask R-CNN [22] with a Multi-Scale Mask-Attended classifier, refining class predictions based on mask-attended features to improve instance segmentation. Recently, with advancements in segmentation techniques utilizing information beyond vision, promptable segmentation models incorporating external prompts, such as text or prototypes, have been proposed for SIS.

SurgicalSAM [17] introduces an efficient fine-tuning method for the Segment Anything Model (SAM) [24], which employs prompts (points, bounding boxes, or text inputs) from a prompt encoder. Since SAM was originally designed for natural domain image segmentation, SurgicalSAM adapts it for the surgical domain. Additionally, it introduces a prototype-based class prompt encoder that generates prompt embeddings for each class as inputs to SAM. Later, various text-promptable SIS methods were proposed, leveraging vision-language models for text-based segmentation. SP-SAM [11] builds upon SAM [24], incorporating both category-level and part-level text prompts. TP-SIS [10], based on CLIP [25], utilizes text prompts describing instruments, categorized into name-based prompts, CLIP’s prompt templates, and prompts generated from GPT-4 [16]. However, these methods assume that the described instrument is always present in the image, leading to incorrect masks when the object is absent. To mitigate this, existing approaches first identify the instruments and then generate prompts based on detected objects.

However, this introduces inaccessible prior information during evaluation, leading to unfair comparisons with vision-only models. We rethink text-promptable SIS by introducing Robust text-promptable SIS (R-SIS), which eliminates this assumption and ensures a fair evaluation. Unlike prior methods that selectively use prompts for detected objects, R-SIS systematically integrates prompts for all classes, allowing the model to infer object presence dynamically. Also, our approach addresses the false positives inherent in previous text-promptable SIS models.

B. Referring Image Segmentation

RIS aims to segment objects based on a given text expression. Early works like MAttNet [13] used language attention networks and object proposals to match expressions with objects. Later methods, such as VLT [26] and EFN [27], employed Bi-GRU language models and ResNet-based encoders to fuse multi-modal information. The adoption of Vision Transformers (ViT) [28] has led to further advancements in RIS. LAVT [12] integrates BERT-based text encoding with visual features from ViT through pixel-word attention, significantly improving segmentation accuracy.

However, a key limitation of prior RIS models is the assumption that every text expression corresponds to an object in the image. This assumption leads to incorrect mask generation when no relevant object is present. Generalized Referring Expression Segmentation [14] tackles this issue by introducing empty-target (no target) and multi-target scenarios. RefSegformer [15] further refines this approach by explicitly handling the empty-target problem, ensuring robust segmentation even when the described object is absent. This empty-target problem

also affects text-promptable SIS methods, where prompts often refer to objects that do not exist in the image. Our work extends robust RIS framework to SIS, addressing false positives while ensuring fair comparisons between promptable and vision-based segmentation models.

III. METHOD

This section presents our approach to R-SIS and RoSIS. Section III-A formulates the problem for R-SIS, identifying the notation and procedure of promptable segmentation for surgical instruments. Section III-B defines the construction of text prompts used for training, detailing the use of descriptive prompts to enhance model understanding. Section III-C describes the architecture of RoSIS, including the encoder-decoder structure and multi-modal fusion components. Finally, Section III-D introduces an iterative refinement strategy aimed at refining mask accuracy through repeated inference steps.

A. Problem formulation

SIS is the task of segmenting surgical tools in an endoscopic surgery image $I \in \mathbb{R}^{H \times W \times 3}$, where H and W denote the height and width of the image, respectively. For text-promptable SIS, we incorporate an image I and a text prompt T containing the names or attributes of the surgical tools, making the segmentation task responsive to specific prompts.

In traditional vision-based SIS, the model takes only image I as input and predicts a mask $M \in \mathbb{R}^{H \times W \times C}$ that includes C classes, each corresponding to a specific surgical instrument. However, in text-promptable SIS, both the image I and a class-specific text prompt t_c are provided as input for each class c . This enables the model to generate a binary mask $M_c \in \mathbb{R}^{H \times W \times 1}$ for each class c . For the R-SIS, we also generate an existence probability p_c , which classifies the class c in the image for a given text prompt t_c .

In the test phase, we conduct inference across all C classes for a given image I , resulting in class-specific masks M_1, \dots, M_C and existence probabilities p_1, \dots, p_C . These outputs are then aggregated to the final mask $M \in \mathbb{R}^{H \times W \times C}$, with each pixel in M representing the class-specific segmentation.

To ensure R-SIS, we incorporate existence probabilities, allowing our model to assess the presence of each instrument class first. This setup enables to avoid producing unnecessary masks for absent classes, reducing false positives, and enhancing segmentation accuracy under the R-SIS setting. By integrating class existence probabilities, our method is evaluated under robust conditions with vision-based models and demonstrates results under practical conditions.

B. Prompt generation

There are various ways to create text prompts t_c for each class c . Following the approach in [10], we generate prompts using the class name, such as “The {cls name}” and we utilize GPT-4 [16] to create detailed prompts describing each class’s visual characteristics and keep them during the train and test phase. This combination provides both general and specific

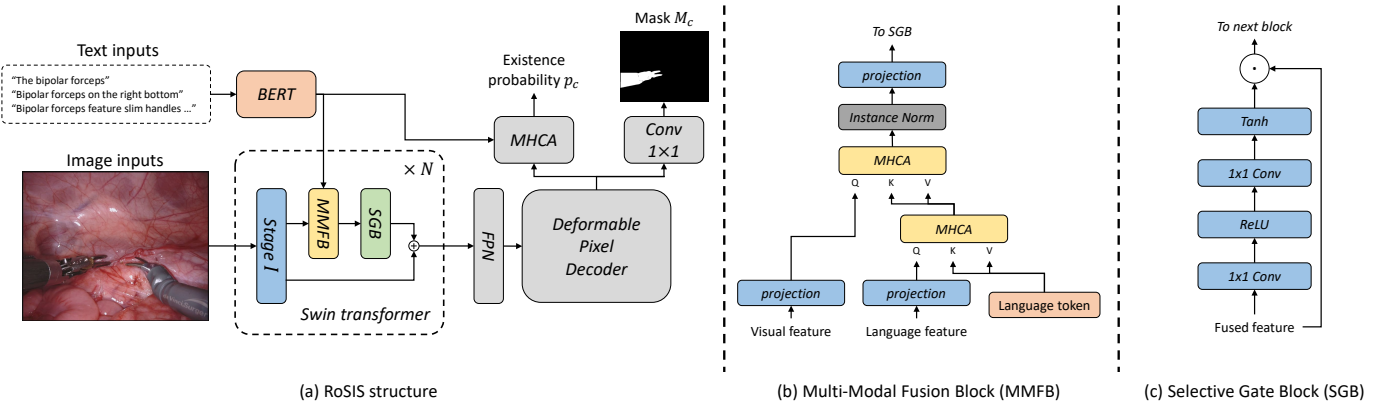


Fig. 3. RoSIS model architecture with (a) overall structure, (b) Multi-Modal Fusion Block, and (c) Selective Gate Block.

prompts, enabling the model to recognize instruments based on both name and appearance.

Since surgical instruments often appear in consistent positions on the screen during surgery, we further enhance the prompts by designing location-based descriptions. To do this, we calculate the center of mass for each instrument’s ground truth mask to identify its typical position, creating prompts like “The {cls name} on the {location}.” For location prompts, we categorize positions into four options: “left-top,” “left-bottom,” “right-top,” and “right-bottom.” During model training, we employ all three types of text prompts—class name prompt, GPT-4 visual prompt, and location prompt—for each class c , ensuring comprehensive contextual information.

If training only with positive prompts (describing objects present in the image), the model may develop a bias toward the presence of instruments, potentially reducing generalization [15]. To counter this, we also generate negative prompts for classes absent from the image, thus enhancing the classification ability to distinguish between existing and non-existing classes. For absent classes, we create prompts using both the class name and GPT-4 description prompts, as well as a randomly selected location prompt from the four options, to provide a full range of negative examples. We balance the positive and negative prompts corresponding to one image for stable training.

C. Architecture

We design our *Robust Surgical Instrument Segmentation (RoSIS)* using an encoder-decoder structure to achieve robust text-promptable SIS. Inspired by [15] and [14], we add a binary classifier in parallel with the decoder to determine the existence of instruments. First, we encode the image I and text description T using an image encoder and a text encoder, respectively. The image encoder is based on the Swin Transformer [29], which is specialized for dense prediction tasks, while the text encoder uses BERT [30]. We denote the visual feature from stage i of the Swin Transformer as $v_i \in \mathbb{R}^{H_i \times W_i \times C_i}$ and the language feature from BERT as $l \in \mathbb{R}^{T \times C_l}$, where H_i and W_i are the height and width of the visual feature, T is the number of words in the text description, and C_i and C_l represent the number of channels for the visual and language features, respectively.

1) Encoder design: We introduce early feature fusion to efficiently integrate vision and language knowledge from the encoder. We aim to enhance semantic understanding and improve feature interactivity through early fusion. For this purpose, we add the *MMFB* and the *SGB* between each stage of the Swin Transformer.

Fig. 3(b) shows the architecture of the *MMFB*, which is designed to integrate visual and language features through a multi-step fusion process, with the fused feature then passed to a gating module. The fusion process begins by independently projecting the visual and language features into compatible feature spaces. The *MMFB* contains two Multi-Head Cross Attention (MHCA) modules. In the first MHCA, we adopt language tokens to fuse with the language feature. The language token is a learnable parameter that adjusts the language feature before the fusion. Unlike [15], since we do not use the language features generated during fusion in the decoder, we focus on selecting only the information necessary for fusion with visual features. Therefore, we refine the language features with the first MHCA and subsequently use them in the second MHCA to interact with the visual features.

Inspired by [12], after the *MMFB*, we introduce the *SGB* to regulate the flow of fused features, ensuring that language features do not dominate the visual information. The *SGB* dynamically controls feature importance, allowing the model to maintain a balanced representation of both visual and language features before passing them to the next stage. As shown in Fig. 3(c), the *SGB* takes the fused feature as input, processes it through a series of lightweight transformations and applies a gating mechanism.

The whole fusion process between each stage are formulated as follows:

$$v_i = V_i(f_{i-1}), \quad i \in \{1, 2, 3, 4\} \quad (1)$$

$$f_i = \begin{cases} v_i + SGB_i(MMFB_i(v_i, l)), & i \in \{1, 2, 3, 4\}, \\ I, & i = 0 \end{cases} \quad (2)$$

where V_i represents the i -th stage of the Swin Transformer, and SGB_i and $MMFB_i$ denote the i -th fusion blocks placed between V_i and V_{i+1} . We describe the effects of the encoder fusion architecture in the ablation study in Table V.

2) Decoder design: Our decoder is designed to perform two tasks: classify the existence of the object specified by

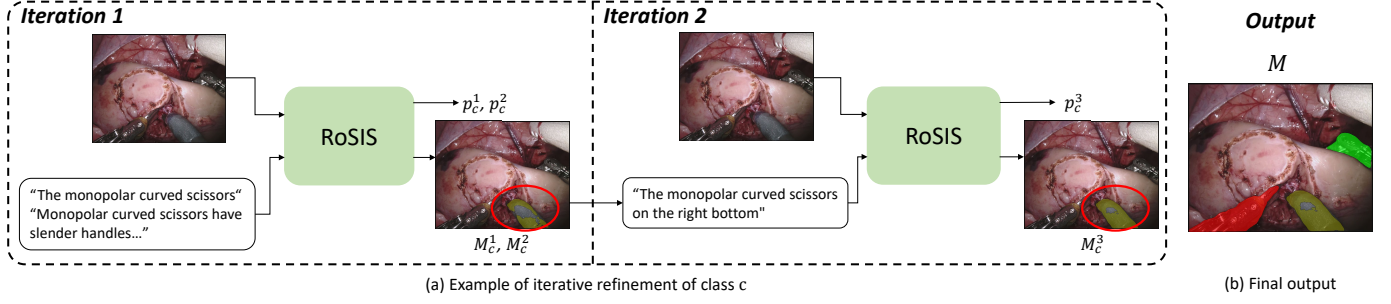


Fig. 4. (a) Iterative refinement process of class c (monopolar curved scissors in this image): (Iteration 1) Initial segmentation using a general prompt, (Iteration 2) refined segmentation with a location prompt referring to the first predicted map. Then, we combine maps by equation 4 for accurate final output. (b) After applying the iterative refinement process to all classes, the refined maps are combined to generate the final output.

the text prompt and generate the corresponding segmentation mask. To accomplish this, we use a multi-scale deformable attention pixel decoder [31]. This decoder incorporates an Feature Pyramid Networks [32] structure to effectively utilize multi-scale features, taking f_1, f_2, f_3 , and f_4 as inputs. The final segmentation mask M_c is produced to pass the output from the decoder through a 1×1 convolution layer.

In addition to mask generation, we introduce a parallel branch to compute the existence probability of the object described by the text prompt. This branch fuses the decoder output from f_4 with the raw language feature extracted from BERT using MHCA. This fusion enables the decoder to leverage both visual and textual information, enhancing its ability to determine the presence of the specified object. Unlike [15], which uses fused language features from the encoder for existence prediction, we use the raw language feature directly from BERT, as it retains richer semantic context. After the fusion through MHCA, the existence probability p_c is computed by passing the output through a linear layer.

Finally, we calculate the cross-entropy loss for both the generated mask and the existence probability to optimize the model's accuracy in both segmentation and existence detection tasks, shown as follows:

$$L = BCELoss(p_c, y_c) + \lambda \cdot CELoss(M_c, M_c^{gt}) \quad (3)$$

where λ is a hyperparameter for mask loss, y_c and M_c^{gt} denote the ground truth of the existence and the mask of class c , respectively.

D. iterative refinement

We propose an *iterative refinement* strategy to use location prompts during inference, similar to those used in training. In the training phase, we can generate location prompts because we have access to the instrument's ground truth, but this is not possible in the inference phase. Therefore, as shown in Fig. 4, we divide the inference process into two iterations.

In the first iteration, we generate the initial segmentation map and existence probability for each instrument category. We use two prompts: a category name prompt (e.g., "The monopolar curved scissors") and a descriptive prompt generated by GPT-4, which provides visual characteristics of the instrument. For category c , the model predicts the segmentation maps M_c^1 and M_c^2 and the existence probabilities p_c^1 and p_c^2 .

If the average existence probability $(p_c^1 + p_c^2)/2$ exceeds 0.5, indicating that class c exists in the image, the process proceeds to the second iteration.

In the second iteration, spatial information is used to refine the segmentation. Based on the segmentation maps M_c^1 and M_c^2 from the first iteration, the model calculates the center of mass for the detected object, allowing it to determine a rough location within one of four quadrants: left-top, left-bottom, right-top, or right-bottom. This positional information is then incorporated into a new location prompt (e.g., "The monopolar curved scissors on the right bottom"), which serves as input for the second inference. The model generates the segmentation map M_c^3 and the existence probability p_c^3 for the class c .

For the final output M_c , the segmentation maps from both iterations are combined using as below:

$$M_c = \begin{cases} 0, & \text{if } \frac{p_c^1 + p_c^2}{2} < 0.5 \\ \frac{M_c^1 + M_c^2}{2}, & \frac{p_c^1 + p_c^2}{2} \geq 0.5 \& p_c^3 < 0.5 \\ \frac{M_c^1 + M_c^2 + M_c^3}{3}, & \frac{p_c^1 + p_c^2}{2} \geq 0.5 \& p_c^3 \geq 0.5 \end{cases} \quad (4)$$

This combination leverages both the fixed prompts and the location prompt, resulting in a more precise and contextually aware segmentation map. This iterative refinement approach ensures robust segmentation by progressively refining predictions based on both textual and spatial prompts, enhancing segmentation performance in complex surgical images. We describe the effects of iterative refinement in detail in the ablation study in Table VII.

IV. EXPERIMENT

A. Dataset and metric

We evaluate our method using the EndoVis2017 [18] and EndoVis2018 [19] datasets based on endoscopic surgery videos. The EndoVis2017 dataset consists of 10 videos recorded using the da Vinci surgical robot system, each containing 255 frames. This dataset includes seven classes: bipolar forceps (BF), prograsp forceps (PF), large needle driver (LND), vessel sealer (VS), grasping retractor (GR), monopolar curved scissors (MCS), and ultrasound probe (UP). Following [3], we apply 4-fold cross-validation to assess performance. The EndoVis2018 dataset consists of 15 videos, divided into 11 training and 4 test video sequences, and includes the

TABLE I
PROMPT INFORMATION FOR EACH CLASS GENERATED FROM GPT-4 [16].

GPT-4 prompt information	
Question	Answer
Question	Please describe the appearance of the {cls name} in endoscopic surgery with 18 words, change the description to a phrase with the subject, and do not use colons and “endoscopic surgery” and “minimally invasive procedure”.
Class name	Answer
Bipolar forceps	Bipolar forceps feature slim insulated handles and precise tips for targeted tissue coagulation and manipulation.
Prograsp forceps	Prograsp forceps feature ergonomic handles and curved serrated jaws for secure and precise tissue manipulation during surgery.
Large needle drivers	Large needle drivers are equipped with sturdy handles and sharp precise jaws for efficient suturing in surgical settings.
Monopolar curved scissors	Monopolar curved scissors have slender ergonomic handles and sharp curved blades for precise cutting during surgical operations.
Ultrasound probe	The ultrasound probe features a slim elongated design with a smooth tip for detailed imaging during surgical interventions.
Suction instrument	The suction instrument boasts a narrow elongated tube with a controllable tip for precise fluid removal during surgery.
Clip applier	The clip applier has a long slender shaft with a specialized tip for deploying clips securely during surgical procedures.
Vessel sealer	Vessel sealer features a streamlined handle and specialized tips for precise sealing and division of blood vessels during surgery.
Grasping retractor	Grasping retractor sports a long handle with claw-like tips for firmly holding tissues during surgical operations.

TABLE II
COMPARISON OF PREVIOUS METHODS IN TERMS OF DOMAIN, INPUT DATA TYPE, AND ROBUSTNESS EVALUATION.

Method	Domain	Input	Robustness
TernausNet-11 [4]	vision	I	clear
TraSeTR [20]	vision	S	clear
MF-TAPNet [5]	vision	S	clear
Dual-MF [6]	vision	S	clear
ISINet [7]	vision	S	clear
MATIS [9]	vision	S	data leakage
S3Net [8]	vision	I	use only top 5 instance
TP-SIS [10]	promptable	I	inaccessible information
RoSIS (ours)	promptable	I	clear

following seven classes: bipolar forceps, prograsp forceps, large needle driver, monopolar curved scissors, ultrasound probe, suction instrument (SI), and clip applier (CA). The EndoVis2018 dataset exhibits severe class imbalance in the training set, and to ensure balanced learning, we adjust class frequencies within the dataloader.

As mentioned in Section III-B, we use three fixed prompts during training for each class. The first prompt incorporates the class name, i.e., “The {cls name},” the second refers to the object’s location, i.e., “The {cls name} on the {location},” and the third prompt is generated from GPT-4. As shown in Table I, the prompts generated by GPT-4 describe the appearance of the class based on its name. During inference, we only use the class name and the GPT-4 prompts, as the location information is not available at the start.

We follow the evaluation metrics used in previous works [7], [10], which include Challenge IoU (Ch IoU), ISI IoU, and mean class IoU (mc IoU). Ch IoU calculates the IoU for classes present in the image and then computes the average. ISI IoU measures the IoU across all classes, while mc IoU represents the average IoU for each class.

B. Implementation detail

We implement our model using PyTorch [33]. For the language model, we utilize a pre-trained BERT [30]. The image encoder is initialized with an ImageNet [34] pre-trained Swin Transformer [29] to support dense prediction. In our fusion module, we set the language token size to 20. The model is trained using the AdamW [35] optimizer with a weight decay of 0.01 for 50 epochs, applying a learning rate decay of 0.1 at epochs 30 and 40. The input images, originally sized at 1280×1024 , are resized to 480×480 for training, and the generated masks are upsampled to their original size to produce the final mask. We train the model with a batch size of 32, using four Nvidia RTX A6000 GPUs.

C. Comparative results

Table II presents a comparison of previous methods in terms of domain, input data type, and robustness evaluation. The domain categorization differentiates between vision-based methods, which rely solely on image features, and promptable methods, which incorporate additional guidance such as textual prompts for segmentation. The input data type column distinguishes methods that operate on a single image (I) from those that leverage a sequence of images (S) to enhance segmentation performance using temporal information. The robustness column indicates whether each method has been evaluated under robust conditions. Methods such as MATIS [9], S3Net [8], and TP-SIS [10] do not meet robustness evaluation criteria due to issues like data leakage or inaccessible information. We exclude MATIS from the comparison methods because it conducts experiments excluding certain videos during the experiment. S3Net uses whole train/test data, but it selects the top 5 instances out of 7 instances during inference. TP-SIS is re-implemented under robust conditions and used in experiments.

In Tables III and IV, we compare our method, RoSIS, with both vision-based and promptable models on the EndoVis2018 [19] and EndoVis 2017 [18] datasets. For a fair comparison,

TABLE III

COMPARISON BETWEEN OUR ROSIS WITH THE PREVIOUS VISION-BASED AND PROMPTABLE METHOD ON THE ENDOVIS2018 DATASET. * MEANS RE-IMPLEMENTED RESULTS. † MEANS INFERENCE UNDER NOT ROBUSTNESS CONDITIONS. **BOLD** AND UNDERLINE INDICATE THE BEST AND THE SECOND BEST PERFORMANCE, RESPECTIVELY.

Domain	Method	Ch IoU	ISI IoU	mc IoU	Instrument category						
					BF	PF	LND	SI	CA	MCS	UP
Vision	TernausNet-11 [4]	46.22	39.87	14.19	44.20	4.67	0.00	0.00	0.00	50.44	0.00
	TraSeTR [20]	76.20	-	47.77	76.30	53.30	46.50	40.60	13.90	86.30	17.50
	MF-TAPNet [5]	67.87	39.14	24.68	69.23	6.10	11.68	14.00	0.91	70.24	0.57
	Dual-MF [6]	70.40	-	35.09	74.10	6.80	<u>46.00</u>	30.10	<u>7.60</u>	80.90	0.00
	ISINet [7]	73.03	70.97	40.21	73.83	48.61	30.98	37.68	<u>0.00</u>	<u>88.16</u>	2.16
	S3Net [†] [8]	75.81	<u>74.02</u>	42.58	77.22	<u>50.87</u>	19.83	50.59	0.00	92.12	7.44
Promptable	LAVT* [12]	72.87	32.58	25.97	77.19	10.96	8.79	16.47	2.78	64.04	1.55
	RefSegformer [15]	<u>77.09</u>	68.67	36.70	<u>80.67</u>	20.88	25.06	38.86	0.10	86.23	5.13
	TP-SIS* [10]	70.55	55.37	29.93	72.12	12.33	15.66	20.56	1.98	85.56	1.30
	RoSIS (ours)	77.66	76.16	<u>44.54</u>	84.11	42.73	<u>35.26</u>	46.36	0.00	88.10	<u>15.22</u>

TABLE IV

COMPARISON BETWEEN OUR ROSIS WITH THE PREVIOUS VISION-BASED AND PROMPTABLE METHOD ON THE ENDOVIS2017 DATASET. * MEANS RE-IMPLEMENTED RESULTS. † MEANS INFERENCE UNDER NOT ROBUSTNESS CONDITIONS. **BOLD** AND UNDERLINE INDICATE THE BEST AND THE SECOND BEST PERFORMANCE, RESPECTIVELY.

Domain	Method	Ch IoU	ISI IoU	mc IoU	Instrument category						
					BF	PF	LND	VS	GR	MCS	UP
Vision	TernausNet-11 [4]	35.27	12.67	10.17	13.45	12.37	20.51	5.97	1.08	1.00	16.76
	TraSeTR [20]	60.40	-	36.79	45.20	56.70	55.80	38.90	<u>11.40</u>	31.30	18.20
	MF-TAPNet [5]	37.35	13.49	10.77	16.39	14.11	19.01	8.11	0.31	4.09	13.40
	Dual-MF [6]	45.80	-	26.40	34.40	21.50	64.30	24.10	0.80	17.90	21.80
	ISINet [7]	55.62	52.20	28.96	38.70	38.50	50.09	27.43	2.01	28.72	12.56
	S3Net [†] [8]	72.54	71.99	46.55	75.08	<u>54.32</u>	<u>61.84</u>	35.50	27.47	<u>43.23</u>	28.38
Promptable	LAVT* [12]	37.57	11.10	10.90	17.05	12.97	14.25	11.91	2.23	7.98	9.90
	RefSegformer [15]	46.58	32.81	27.87	33.37	0.30	52.69	38.50	0.03	37.05	<u>33.14</u>
	TP-SIS* [10]	51.36	46.64	31.24	43.81	27.70	46.42	<u>41.25</u>	3.98	46.83	8.70
	RoSIS (ours)	<u>63.07</u>	<u>57.33</u>	<u>40.65</u>	<u>67.34</u>	39.95	55.85	45.32	5.10	26.00	44.99

we re-implement the promptable models LAVT [12] and TP-SIS [10], both of which are based on referring image segmentation tasks. For promptable methods, we provide referring sentences for all classes in the dataset. Pixel-wise probabilities of the generated masks were then compared to produce the final output.

1) *Comparison on the EndoVis2018*: As shown in Table III, RoSIS outperforms all promptable segmentation models and achieves superior performance over vision-based methods in Ch IoU, ISI IoU, and mc IoU. S3Net is the strongest vision-based model in ISI IoU that utilizes a single image. However, RoSIS surpasses it under robust conditions, improving Ch IoU by +2.44%, ISI IoU by +2.89%, and mc IoU by +4.60%. Meanwhile, TraSeTR, which achieves the highest mc IoU among vision-based models, benefits from using sequential images instead of single-image inference. Despite this advantage, RoSIS remains competitive while relying solely on single-image processing.

Compared to promptable models like LAVT and TP-SIS, RoSIS effectively reduces false positives and false negatives. Existing promptable methods generate segmentation masks without first verifying object existence, causing a noticeable gap between Ch IoU and ISI IoU scores. In contrast, RoSIS incorporates an existence verification step, stabilizing the

TABLE V
TEXT PROMPT DESIGN AND ITERATIVE REFINEMENT ABLATION STUDY
IN ENDOVIS2018 DATASET. THE VALUES IN BRACKETS REPRESENT
THE INCREASE COMPARED TO THE BASELINE.

	ISI IoU	Ch IoU	mc IoU
Name prompt	67.74	76.20	37.84
(+) location prompt	69.24	76.57	37.54
(+) iterative refinement	73.51	77.58	39.30
(+) GPT-4 prompt	71.37	77.21	40.61
(+) iterative refinement	76.16	77.66	44.54

segmentation process by minimizing false negatives. This refinement results in higher segmentation accuracy, making RoSIS a more reliable solution for robust surgical instrument segmentation.

2) *Comparison on the EndoVis2017*: Table IV presents a comparison between RoSIS and previous vision-based and promptable methods on the EndoVis2017 [18] dataset. Among the vision-based methods, S3Net [8] achieves the highest performance, surpassing RoSIS on this dataset. However, S3Net's inference is constrained by a selective approach, considering only the top 5 instances, which can lead to an unfair comparison by potentially omitting relevant objects. While this

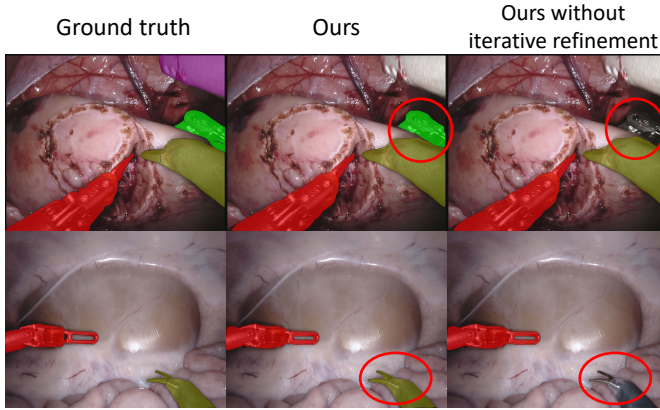


Fig. 5. Visual comparison of iterative refinement strategies

TABLE VI

A VISUAL AND LANGUAGE FEATURE FUSION STRUCTURAL ABLATION STUDY AND PERFORMANCE COMPARISON OF THE FUSION STRUCTURE ON THE ENDOVIS2018 DATASET. WE CHECK THE PERFORMANCE OF EACH MODULE, INCLUDING MMFB, SGB, RAW LANGUAGE FEATURES (RL), AND LANGUAGE TOKEN (LT).

Method	MMFB	SGB	RL	LT	ISI IoU	Ch IoU	mc IoU
Ours	✓	✗	✗	✗	64.31	72.75	34.27
	✓	✓	✗	✗	71.65	77.07	38.23
	✓	✓	✓	✗	74.36	80.37	41.87
	✓	✓	✓	✓	76.16	77.66	44.54
VLTF (RefSegformer) [15]					68.58	74.19	33.48
PWAM (LAVT) [12]					66.94	79.34	36.89

restriction may enhance performance, it limits applicability in real-world scenarios where all relevant instruments must be segmented.

Moreover, RoSIS outperforms other vision-based and promptable models while maintaining a more balanced class-wise performance distribution. Notably, its ISI IoU shows less performance degradation compared to Ch IoU, highlighting the effectiveness of its fusion structure, prompt design, and iterative refinement strategy. Even under robust conditions, RoSIS achieves superior performance in two key instrument categories: VS and UP. These results further validate RoSIS's ability to effectively integrate vision-based and promptable features, making it a versatile and efficient solution for surgical instrument segmentation.

D. Ablation study

1) *Iterative refinement process and prompt design:* Table V presents the ablation study results on the EndoVis2018 dataset, emphasizing the role of iterative refinement and text prompts. Starting with the baseline using only the name prompt such as "The bipolar forceps," the model achieves ISI IoU and mc IoU scores of 67.74 and 37.84, respectively. Adding the location prompt to the name prompt slightly improves performance in ISI IoU. Then, the iterative refinement consistently improves performance across all metrics. This demonstrates that iterative refinement effectively refines the segmentation map by utilizing location-specific prompts, contributing to more

accurate segmentation. Similarly, when iterative refinement is incorporated with the GPT-4 prompt, which provides descriptive characteristics for each instrument, there is a substantial improvement in segmentation accuracy. The ISI IoU increases by 4.79, and mc IoU increases by 3.93. This improvement shows the synergy between descriptive prompts and iterative refinement, as the iterative process allows the model to refine segmentation based on more detailed object information. Also, as shown in the red circle part of Fig. 5, iterative refinement allows for more accurate object segmentation maps.

These results indicate the crucial role of iterative refinement in our model. By refining segmentation through multiple stages and adapting prompts based on previous outputs, iterative refinement contributes to significant gains in both general and class-specific accuracy, making it a key factor in achieving optimal segmentation performance.

2) *Structure design:* To evaluate the effectiveness of our visual-language fusion structure, we conduct an ablation study on the EndoVis2018 dataset, analyzing the impact of each module on segmentation performance. Specifically, we assess the contributions of the Multi-Modal Fusion Block (MMFB), Selective Gate Block (SGB), Raw Language features (RL), and Language Token (LT) by incrementally adding components to our framework. RL involves using language features extracted from BERT [30] directly as input for the MHCA module in the existence prediction branch, enhancing textual representation within our segmentation framework. The results are summarized in Table VI.

Our findings demonstrate that each proposed module contributes to segmentation performance. SGB improves segmentation stability by selectively refining the fusion of visual and language features. RL enhances the model's ability to process textual information, leading to slight improvements in segmentation accuracy. LT further strengthens feature representation, helping the model to refine segmentation masks more effectively. When combined, these modules achieve the best overall performance, validating their role in improving segmentation robustness.

To evaluate the effectiveness of our fusion structure, we compare our model with previous RIS methods, including VLTF (RefSegformer) [15] and PWAM (LAVT) [12]. The results show that our method improves segmentation accuracy and maintains stable performance. Unlike previous methods that rely heavily on either vision or language cues, our approach balances multi-modal information more effectively, reducing misclassification and false positives. The consistent improvement across key metrics confirms its robustness and reliability in surgical instrument segmentation.

E. Qualitative results

In Fig. 6, we visualize the prediction of our model, the ground truth, and the other promptable segmentation methods [10], [12]. Since other methods are trained without robust conditions, they hard to determine the presence or absence of objects in the R-SIS environment, resulting in higher false positives in the predicted maps. As shown in the 4th and 5th columns of Fig. 6, the segmentation masks for various classes

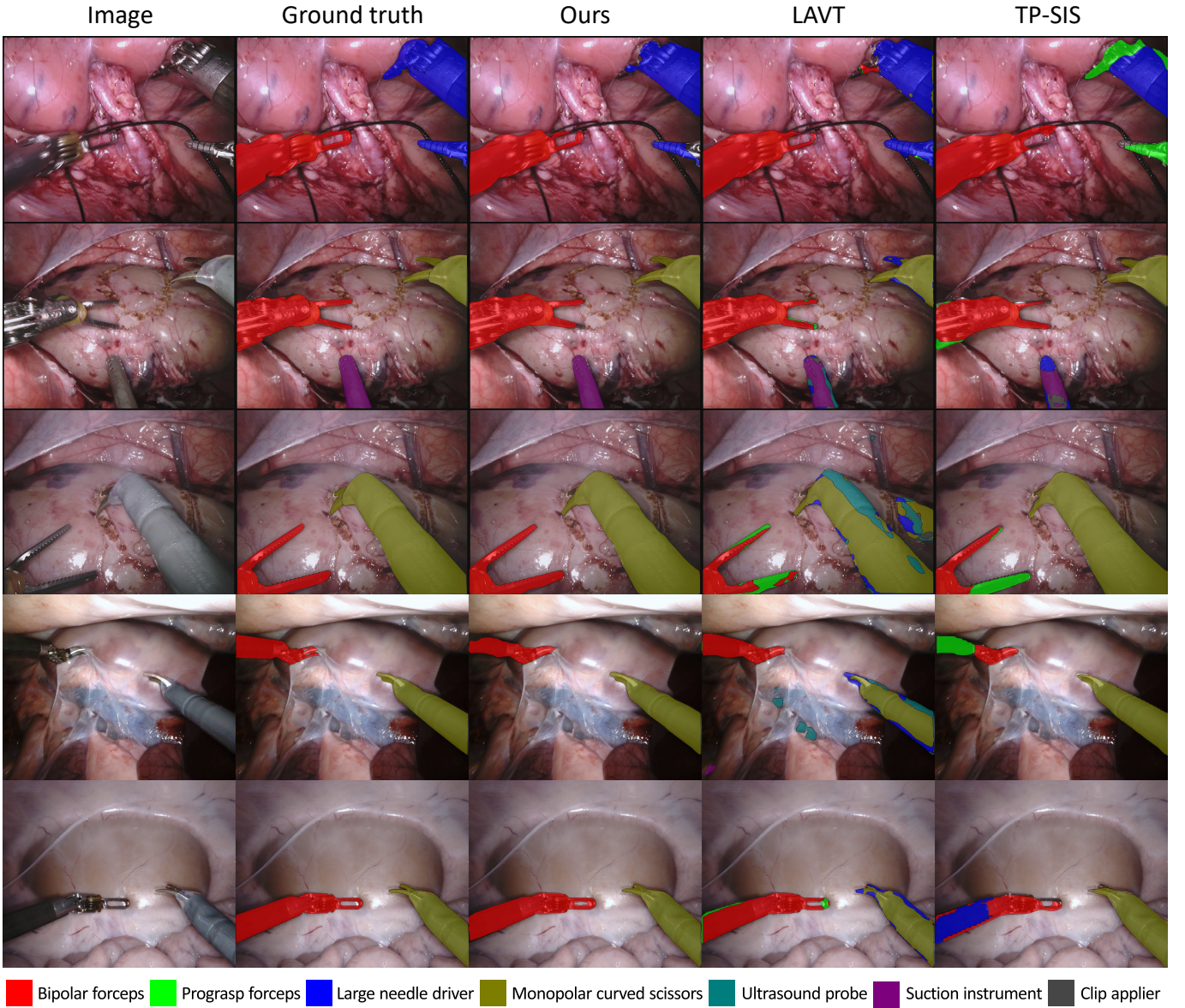


Fig. 6. Qualitative results of our predicted maps, the ground truth masks, and other promptable segmentation methods from the EndoVis2018 validation set.

overlap. This overlap occurs because segmentation maps are generated for all classes' text prompts, causing all maps to merge. In contrast, our model first verifies the presence or absence of an object before generating a map, producing a clean segmentation for a single object and leading to a low false positive rate, which is crucial in surgical environments.

F. Cross-dataset study

We also evaluate our method in a cross-dataset setting. In this setup, the model is trained on the EndoVis2018 dataset and tested on the EndoVis2017 dataset, and vice versa. The EndoVis2017 and EndoVis2018 datasets share five common categories and each includes two unique categories. As shown in Table VII, RoSIS demonstrates better performance compared to other promptable segmentation methods. Additionally, even among shared categories, there are slight differences

TABLE VII
CROSS-DATASET SETTING PERFORMANCE COMPARISON BY TRAINING
ON THE ENDOVIS2018 AND TESTING ON THE ENDOVIS2017, AND
VICE VERSA.

Setting	Method	Ch IoU	ISI IoU	mc IoU
EV18→EV17	LAVT [12]	40.82	14.35	13.26
	TP-SIS [10]	34.23	18.57	20.16
	RoSIS (ours)	42.45	34.67	27.68
EV17→EV18	LAVT [12]	46.57	15.67	14.91
	TP-SIS [10]	37.81	26.72	14.93
	RoSIS (ours)	58.31	51.00	23.99

in shape and domain variations, making the cross-dataset experiment indicate the generalizability of methods.

The promptable segmentation methods LAVT [12] and TP-SIS [10] show overall lower performance, with a large discrep-

ancy between their Ch IoU and ISI IoU scores. In contrast, our method, RoSIS, achieves the best results, with a smaller gap between Ch IoU and ISI IoU, showing its robustness and efficiency. These results demonstrate the generalizability and effectiveness of RoSIS in handling domain shifts across different datasets.

V. CONCLUSION

In this work, we redefined the task of text-promptable Surgical Instrument Segmentation (SIS) under robust conditions as Robust text-promptable SIS (R-SIS). Existing methods often assume the presence of objects described by prompts, leading to challenges in realistic surgical scenarios. Such assumptions introduce biases in evaluation, as they leverage prior object knowledge that is not available to vision-based models. R-SIS eliminates this dependency by enforcing prompt-based segmentation without prior knowledge of object presence. This ensures fairer comparisons between promptable and vision-based methods while improving robustness in real-world surgical applications.

To optimize model performance for R-SIS, we introduce Robust Surgical Instrument Segmentation (RoSIS), a novel framework designed to enhance segmentation robustness and accuracy. RoSIS employs an encoder-decoder architecture with MMFB and SGB to achieve a balanced integration of visual and language features, preventing the dominance of either modality. Additionally, we introduced an iterative refinement strategy to refine segmentation maps, utilizing both name-based and location-based prompts to improve accuracy.

Our experiments on the EndoVis2017 and EndoVis2018 datasets demonstrated that RoSIS outperforms existing vision-based and promptable methods under robust conditions. Ablation studies further validated the effectiveness of our fusion structures, as well as the iterative refinement approach, confirming RoSIS's adaptability across diverse surgical scenarios. This work lays a foundation for future research in multimodal SIS, with applications in other areas where vision-language integration is essential for complex surgical scene understanding.

REFERENCES

- [1] K. Fuchs, "Minimally invasive surgery," *Endoscopy*, vol. 34, no. 02, pp. 154–159, 2002.
- [2] A. G. Harrell and B. T. Hemiford, "Minimally invasive abdominal surgery: lux et veritas past, present, and future," *The American journal of surgery*, vol. 190, no. 2, pp. 239–243, 2005.
- [3] A. A. Shvets, A. Raklin, A. A. Kalinin, and V. I. Iglovikov, "Automatic instrument segmentation in robot-assisted surgery using deep learning," in *2018 17th IEEE international conference on machine learning and applications (ICMLA)*. IEEE, 2018, pp. 624–628.
- [4] V. Iglovikov and A. Shvets, "Ternausnet: U-net with vgg11 encoder pre-trained on imagenet for image segmentation," *arXiv preprint arXiv:1801.05746*, 2018.
- [5] Y. Jin, K. Cheng, Q. Dou, and P.-A. Heng, "Incorporating temporal prior from motion flow for instrument segmentation in minimally invasive surgery video," in *Medical Image Computing and Computer Assisted Intervention–MICCAI 2019: 22nd International Conference, Shenzhen, China, October 13–17, 2019, Proceedings, Part V 22*. Springer, 2019, pp. 440–448.
- [6] Z. Zhao, Y. Jin, X. Gao, Q. Dou, and P.-A. Heng, "Learning motion flows for semi-supervised instrument segmentation from robotic surgical video," in *Medical Image Computing and Computer Assisted Intervention–MICCAI 2020: 23rd International Conference, Lima, Peru, October 4–8, 2020, Proceedings, Part III 23*. Springer, 2020, pp. 679–689.
- [7] C. González, L. Bravo-Sánchez, and P. Arbelaez, "Isinet: an instance-based approach for surgical instrument segmentation," in *International Conference on Medical Image Computing and Computer-Assisted Intervention*. Springer, 2020, pp. 595–605.
- [8] B. Baby, D. Thapar, M. Chasma, T. Banerjee, K. Dargan, A. Suri, S. Banerjee, and C. Arora, "From forks to forceps: A new framework for instance segmentation of surgical instruments," in *Proceedings of the IEEE/CVF winter conference on applications of computer vision*, 2023, pp. 6191–6201.
- [9] N. Ayobi, A. Pérez-Rondón, S. Rodríguez, and P. Arbeláez, "Matis: Masked-attention transformers for surgical instrument segmentation," in *2023 IEEE 20th International Symposium on Biomedical Imaging (ISBI)*. IEEE, 2023, pp. 1–5.
- [10] Z. Zhou, O. Alabi, M. Wei, T. Vercauteren, and M. Shi, "Text promptable surgical instrument segmentation with vision-language models," *Advances in Neural Information Processing Systems*, vol. 36, pp. 28611–28623, 2023.
- [11] W. Yue, J. Zhang, K. Hu, Q. Wu, Z. Ge, Y. Xia, J. Luo, and Z. Wang, "Part to whole: Collaborative prompting for surgical instrument segmentation," *arXiv preprint arXiv:2312.14481*, 2023.
- [12] Z. Yang, J. Wang, Y. Tang, K. Chen, H. Zhao, and P. H. Torr, "Lavt: Language-aware vision transformer for referring image segmentation," in *Proceedings of the IEEE/CVF Conference on Computer Vision and Pattern Recognition*, 2022, pp. 18155–18165.
- [13] L. Yu, Z. Lin, X. Shen, J. Yang, X. Lu, M. Bansal, and T. L. Berg, "Mattnet: Modular attention network for referring expression comprehension," in *Proceedings of the IEEE conference on computer vision and pattern recognition*, 2018, pp. 1307–1315.
- [14] C. Liu, H. Ding, and X. Jiang, "Gres: Generalized referring expression segmentation," in *Proceedings of the IEEE/CVF conference on computer vision and pattern recognition*, 2023, pp. 23592–23601.
- [15] J. Wu, X. Li, X. Li, H. Ding, Y. Tong, and D. Tao, "Towards robust referring image segmentation," *IEEE Transactions on Image Processing*, 2024.
- [16] J. Achiam, S. Adler, S. Agarwal, L. Ahmad, I. Akkaya, F. L. Aleman, D. Almeida, J. Altenschmidt, S. Altman, S. Anadkat *et al.*, "Gpt-4 technical report," *arXiv preprint arXiv:2303.08774*, 2023.
- [17] W. Yue, J. Zhang, K. Hu, Y. Xia, J. Luo, and Z. Wang, "Surgicalsam: Efficient class promptable surgical instrument segmentation," in *Proceedings of the AAAI Conference on Artificial Intelligence*, vol. 38, no. 7, 2024, pp. 6890–6898.
- [18] M. Allan, A. Shvets, T. Kurmann, Z. Zhang, R. Duggal, Y.-H. Su, N. Rieke, I. Laina, N. Kalavakonda, S. Bodenstedt *et al.*, "2017 robotic instrument segmentation challenge," *arXiv preprint arXiv:1902.06426*, 2019.
- [19] M. Allan, S. Kondo, S. Bodenstedt, S. Leger, R. Kadkhodamohammadi, I. Luengo, F. Fuentes, E. Flouty, A. Mohammed, M. Pedersen *et al.*, "2018 robotic scene segmentation challenge," *arXiv preprint arXiv:2001.11190*, 2020.
- [20] Z. Zhao, Y. Jin, and P.-A. Heng, "Trasetr: track-to-segment transformer with contrastive query for instance-level instrument segmentation in robotic surgery," in *2022 International conference on robotics and automation (ICRA)*. IEEE, 2022, pp. 11186–11193.
- [21] O. Ronneberger, P. Fischer, and T. Brox, "U-net: Convolutional networks for biomedical image segmentation," in *Medical image computing and computer-assisted intervention–MICCAI 2015: 18th international conference, Munich, Germany, October 5–9, 2015, proceedings, part III 18*. Springer, 2015, pp. 234–241.
- [22] K. He, G. Gkioxari, P. Dollár, and R. Girshick, "Mask r-cnn," in *Proceedings of the IEEE international conference on computer vision*, 2017, pp. 2961–2969.
- [23] B. Cheng, I. Misra, A. G. Schwing, A. Kirillov, and R. Girdhar, "Masked-attention mask transformer for universal image segmentation," in *Proceedings of the IEEE/CVF conference on computer vision and pattern recognition*, 2022, pp. 1290–1299.
- [24] A. Kirillov, E. Mintun, N. Ravi, H. Mao, C. Rolland, L. Gustafson, T. Xiao, S. Whitehead, A. C. Berg, W.-Y. Lo *et al.*, "Segment anything," in *Proceedings of the IEEE/CVF International Conference on Computer Vision*, 2023, pp. 4015–4026.
- [25] A. Radford, J. W. Kim, C. Hallacy, A. Ramesh, G. Goh, S. Agarwal, G. Sastry, A. Askell, P. Mishkin, J. Clark *et al.*, "Learning transferable

visual models from natural language supervision,” in *International conference on machine learning*. PMLR, 2021, pp. 8748–8763.

[26] H. Ding, C. Liu, S. Wang, and X. Jiang, “Vision-language transformer and query generation for referring segmentation,” in *Proceedings of the IEEE/CVF International Conference on Computer Vision*, 2021, pp. 16 321–16 330.

[27] G. Feng, Z. Hu, L. Zhang, and H. Lu, “Encoder fusion network with co-attention embedding for referring image segmentation,” in *Proceedings of the IEEE/CVF Conference on Computer Vision and Pattern Recognition*, 2021, pp. 15 506–15 515.

[28] A. Dosovitskiy, “An image is worth 16x16 words: Transformers for image recognition at scale,” *arXiv preprint arXiv:2010.11929*, 2020.

[29] Z. Liu, Y. Lin, Y. Cao, H. Hu, Y. Wei, Z. Zhang, S. Lin, and B. Guo, “Swin transformer: Hierarchical vision transformer using shifted windows,” in *Proceedings of the IEEE/CVF international conference on computer vision*, 2021, pp. 10 012–10 022.

[30] J. Devlin, “Bert: Pre-training of deep bidirectional transformers for language understanding,” *arXiv preprint arXiv:1810.04805*, 2018.

[31] X. Zhu, W. Su, L. Lu, B. Li, X. Wang, and J. Dai, “Deformable detr: Deformable transformers for end-to-end object detection,” *arXiv preprint arXiv:2010.04159*, 2020.

[32] T.-Y. Lin, P. Dollár, R. Girshick, K. He, B. Hariharan, and S. Belongie, “Feature pyramid networks for object detection,” in *Proceedings of the IEEE conference on computer vision and pattern recognition*, 2017, pp. 2117–2125.

[33] A. Paszke, S. Gross, F. Massa, A. Lerer, J. Bradbury, G. Chanan, T. Killeen, Z. Lin, N. Gimelshein, L. Antiga *et al.*, “Pytorch: An imperative style, high-performance deep learning library,” *Advances in neural information processing systems*, vol. 32, 2019.

[34] J. Deng, W. Dong, R. Socher, L.-J. Li, K. Li, and L. Fei-Fei, “Imagenet: A large-scale hierarchical image database,” in *2009 IEEE conference on computer vision and pattern recognition*. Ieee, 2009, pp. 248–255.

[35] I. Loshchilov, “Decoupled weight decay regularization,” *arXiv preprint arXiv:1711.05101*, 2017.